

# Generational Spreading Speed and the Dynamics of Population Range Expansion

Andrew W. Bateman,<sup>1,2,\*</sup> Michael G. Neubert,<sup>3</sup> Martin Krkošek,<sup>2</sup> and Mark A. Lewis<sup>1</sup>

1. Department of Biological Sciences and Department of Mathematical and Statistical Sciences, University of Alberta, Edmonton, Alberta T6G 2E9, Canada; 2. Department of Ecology and Evolutionary Biology, University of Toronto, Toronto, Ontario M5S 3B2, Canada; and Salmon Coast Field Station, Simoom Sound, British Columbia V0P 1S0, Canada; 3. Biology Department, Woods Hole Oceanographic Institution, Woods Hole, Massachusetts 02543

Submitted January 5, 2015; Accepted March 4, 2015; Electronically published August 6, 2015

Online enhancement: appendix.

**ABSTRACT:** Some of the most fundamental quantities in population ecology describe the growth and spread of populations. Population dynamics are often characterized by the annual rate of increase,  $\lambda$ , or the generational rate of increase,  $R_0$ . Analyses involving  $R_0$  have deepened our understanding of disease dynamics and life-history complexities beyond that afforded by analysis of annual growth alone. While range expansion is quantified by the annual spreading speed, a spatial analog of  $\lambda$ , an  $R_0$ -like expression for the rate of spread is missing. Using integrodifference models, we derive the appropriate generational spreading speed for populations with complex (stage-structured) life histories. The resulting measure, relevant to locations near the expanding edge of a (re)colonizing population, incorporates both local population growth and explicit spatial dispersal rather than solely growth across a population, as is the case for  $R_0$ . The calculations for generational spreading speed are often simpler than those for annual spreading speed, and analytic or partial analytic solutions can yield insight into the processes that facilitate or slow a population's spatial spread. We analyze the spatial dynamics of green crabs, sea otters, and teasel as examples to demonstrate the flexibility of our methods and the intuitive insights that they afford.

**Keywords:** generational spreading speed, stage structure, invasion speed, integrodifference models, recolonization, net reproductive number, graph reduction, next-generation operator.

## Introduction

Spatial patterns of population growth and spread have long occupied biologists (e.g., Fisher 1937; Elton 1958; Clark 1998), and understanding these patterns is particularly important in the face of mounting human-induced environmental change. Spatial dynamics have direct impacts on the viability of species affected by anthropogenic change (e.g., Potapov and Lewis 2004; Leroux et al. 2013),

the cost of controlling invasive species (e.g., Fagan et al. 2002), and the success of species reintroductions (e.g., Krkošek et al. 2007; Tinker et al. 2008).

A population's rate of range expansion, or spreading speed, is a basic descriptive statistic in spatial ecology, akin to the intrinsic rate of population increase,  $\lambda$ , in discrete-time demographic models (Neubert and Caswell 2000). Estimates of spreading speed and its sensitivity to changes in demographic parameters can help identify promising targets for conservation efforts and biological control (Neubert and Parker 2004). For example, Neubert and Parker (2004) were able to verify the lack of an Achilles' heel life stage for control of leguminous Scotch broom, *Cytisus scoparius*, and Tinker et al. (2008) identified the importance of adult survival in maintaining the coastline recolonization rate for the California sea otter, *Enhydra lutris nereis*.

While  $\lambda$  quantifies geometric population growth between successive time steps (usually years), another statistic— $R_0$ , the net reproductive number—quantifies the expected number of offspring produced by an individual over its lifetime or, equivalently, geometric population growth between generations (Cushing and Yicang 1994; Caswell 2001). These quantities represent foundational concepts in population biology, and the closely associated version of  $R_0$  from epidemiology has even been called “the most important quantity in the study of epidemics” (Heesterbeek 2002, p. 189). While  $\lambda$  and  $R_0$  are equivalent in discrete-time demographic models with nonoverlapping generations, it is more common that generations overlap, creating a nontrivial relationship between the two statistics. Populations can even have the same value of  $\lambda$  and different values of  $R_0$  or vice versa.

Knowing both  $R_0$  and  $\lambda$  improves understanding of a population's demography, and both are indicators of population growth or decline (Cushing and Yicang 1994). At times,  $\lambda$  has no closed-form solution and must be calculated numerically (de-Camino-Beck and Lewis 2007), whereas  $R_0$  is often simpler to calculate, and the ability

\* Corresponding author; e-mail: andrew.w.bateman@gmail.com.

Am. Nat. 2015. Vol. 186, pp. 362–375. © 2015 by The University of Chicago. 0003-0147/2015/18603-55\$15.00. All rights reserved.  
DOI: 10.1086/682276

to derive closed-form expressions offers the potential for greater analytical insight (Caswell 2001; de-Camino-Beck and Lewis 2007; see “Order of the Characteristic Equation” below). For example, de-Camino-Beck and Lewis (2007) showed how an expression for  $R_0$  could be used to explore the biocontrol susceptibility of different life stages of invasive wild teasel, *Dipsacus fullonum* (syn. *D. sylvestris*), gaining an intuition for management that was not readily afforded by numerical analyses of annual population growth rates.

Over the past decades, integrodifference equation (IDE) models, combining discrete-time descriptions of demography with continuous descriptions of spatial movement, have emerged as useful tools for studying spatial population dynamics (Kot et al. 1996; Neubert and Caswell 2000; Krkošek et al. 2007; de-Camino-Beck and Lewis 2009; Bullock et al. 2012). Both stage-structured and scalar (single-stage) demographic submodels have been used, and movement submodels are highly flexible (Kot et al. 1996; Neubert and Caswell 2000; Lutscher 2007). In many cases, integrodifference models allow calculation of a population’s potential spreading speed on the basis of measured demographic rates and individual dispersal propensity (Weinberger 1982; Lui 1989a; Kot et al. 1996; Neubert and Caswell 2000). The approach offers a useful tool for studies and management of species invasion (e.g., by exploring control susceptibility of different life stages; Neubert and Parker 2004), recolonization (e.g., by identifying key processes that may slow spread; Tinker et al. 2008), and spread in a changing climate (e.g., by assessing how changing weather patterns will affect the ability of plants to track shifting climate windows; Zhang et al. 2011; Bullock et al. 2012).

Motivated by the simpler calculations and greater insight afforded by generational measures in demography, we consider generation-by-generation spread in integrodifference models that incorporate stage-structured population dynamics, seeking an analog to  $R_0$  in the context of population spread. We consider space as one dimensional, modeling spread along a roadside, river, or coastline, but note that there are methods to expand our results to two dimensions (Lewis et al. 2006; de-Camino-Beck and Lewis 2009). While our approach is partially inspired by the invasive species literature (Neubert and Caswell 2000; Neubert and Parker 2004) and we retain related terminology at times, our results apply equally to other scenarios, such as reintroductions and translocations, for which spreading speed is a relevant concept.

First, we briefly summarize past results concerning spreading speed and generational population growth. We go on to derive an expression for “generational” spreading speed and explore its relationship to the standard measure. We show how to calculate generational spreading speed and highlight cases in which this can be done analytically, pro-

viding empirical examples that illustrate some practical benefits of the theory. Compared with the standard measure of spreading speed, our measure is an equivalent indicator of whether a species will spread, but its calculation is often simpler. We expect our concept to provide useful insight, for example, into management strategies that could halt an invader’s spread or facilitate a successful reintroduction.

### Standard Spreading Speed

In many biologically relevant cases, IDEs can be used to predict a population’s time-step-by-time-step spreading speed (e.g., for plants: Neubert and Caswell 2000; Neubert and Parker 2004; Bullock et al. 2012; for animals: Krkošek et al. 2007; Tinker et al. 2008; Miller et al. 2011). Stage-structured population models are most commonly built on an annual timescale. To simplify discussion, we refer to annual spread and speed rather than time-step-by-time-step spread and speed, but bear in mind that an annual timescale is inappropriate for some species.

IDEs incorporate species’ underlying demography and dispersal tendencies by considering traveling-wave solutions to a linearized model (Weinberger 1982; Lui 1989a; Neubert and Caswell 2000). We summarize key results here and give a more thorough background in the appendix (available online; “Mathematical Background”).

Stage-structured IDEs model changes to a vector of stage-specific population densities,  $\mathbf{n}(y, t) = [n_1(y, t), \dots, n_N(y, t)]^T$ , measured across locations,  $y$ , in year  $t$ . At the population’s low-density “spreading front,” a linearized, density-independent population projection matrix,  $\mathbf{A}$ , captures demographic changes (Neubert and Caswell 2000; Caswell 2001). Assuming a homogeneous environment, a matrix of dispersal kernels,  $\mathbf{K}(x - y)$ , describes the likelihood that individuals disperse from  $y$  to  $x$  between year  $t$  and  $t + 1$ . Each entry of  $\mathbf{K}(x - y)$ ,  $k_{ij}(x - y)$ , is associated with transition from stage  $j$  to stage  $i$  ( $i, j \in \mathbb{N}$ ). The model components combine to describe spatial dynamics:

$$\mathbf{n}(x, t + 1) = \int_{-\infty}^{\infty} [\mathbf{K}(x - y) \circ \mathbf{A}] \mathbf{n}(y, t) dy, \quad (1)$$

where the open circle ( $\circ$ ) denotes the Hadamard (element-wise) product.

When a species’ life history is conventional, its population grows at low density, population dynamics are negatively density dependent, and dispersal is exponentially bounded, limiting exponential-form traveling-wave solutions take the form

$$\mathbf{n}(x, t) = \mathbf{w} e^{-s(x-ct)}, \quad (2)$$

where  $\mathbf{w}$  describes stage-specific abundances in the wave,  $s$  is the wave shape (or “steepness”) of the spreading front,

and  $c$  is the wave speed (Neubert and Caswell 2000). The annual spreading speed in the positive  $x$ -direction for the density-dependent model is

$$c^* = \min_{s \in \Omega} \left[ \frac{1}{s} \ln(\rho_1[\mathbf{H}(s)]) \right], \quad (3)$$

where  $\mathbf{H}(s) = \mathbf{M}(s) \circ \mathbf{A}$ ,  $\rho_1[\cdot]$  denotes the dominant eigenvalue of a matrix (for most demographic cases, this will be a positive scalar [see “Mathematical Background” in the appendix], and  $\mathbf{M}(s)$  is the matrix of moment-generating functions,  $m_{ij}(s)$ , corresponding to the kernels,  $k_{ij}(x - y)$  (Lui 1989a; Neubert and Caswell 2000). The population spreading at speed  $c^*$  has shape  $s^*$ , meaning that the population density decays as  $e^{-s^*x}$  at the leading edge of the spreading population.

Formulas exist to calculate the sensitivity and elasticity of  $c^*$  to model parameters (Neubert and Caswell 2000). As a result, IDEs can reveal causes of variation in spreading speed related to dispersal and demographic features of a species or landscape (e.g., Neubert and Caswell 2000; Neubert and Parker 2004; Tinker et al. 2008).

#### *Measures of Population Growth*

The spreading speed,  $c^*$ , has nonspatial analog  $\lambda$ , the density-independent asymptotic population growth rate for a stage-structured population, given by the dominant eigenvalue of the population projection matrix,  $\mathbf{A}$  (Caswell 2001). Calculating  $\lambda$  and its sensitivity to demographic parameters has offered insight into population-level patterns (e.g., Shea and Kelly 1998; Parker 2000), much as spreading-speed calculations can offer insight into invasions.

An alternative to calculating  $\lambda$  is to calculate  $R_0$ . Called the net reproductive number,  $R_0$  represents a population’s generational growth rate (Caswell 2001). To calculate  $R_0$ , we first decompose  $\mathbf{A}$  into stage-specific transition and fecundity matrices,  $\mathbf{T}$  and  $\mathbf{F}$ , respectively (see “Mathematical Background” in the appendix).  $R_0$  is the dominant eigenvalue of the next-generation matrix,  $\mathbf{Q} = \mathbf{F}[\mathbf{I} - \mathbf{T}]^{-1}$  (Cushing and Yicang 1994; Caswell 2001; Li and Schneider 2002).

Like  $\lambda$ , the value of  $R_0$  indicates whether the abundance of individuals in a given population will increase or decrease. One of three cases is possible:

$$0 \leq R_0 \leq \lambda < 1, \quad R_0 = \lambda = 1, \quad \text{or} \quad 1 < \lambda \leq R_0, \quad (4)$$

corresponding to population decline, equilibrium, or growth, respectively (Cushing and Yicang 1994; Li and Schneider 2002). Not only does statement (4) indicate that  $(R_0 - 1)$  and  $(\lambda - 1)$  have the same sign, it indicates an ordering between  $R_0$  and  $\lambda$  for both growing ( $R_0 > \lambda$ ) and declining ( $R_0 < \lambda$ ) populations. We explore an analogous situation in the context of biological invasion.

In seeking a generational measure of spreading speed, we are motivated by an observation from analogous non-spatial demographic models. Often,  $\mathbf{F}$  takes a special form: when all reproduction is by a single adult stage or all offspring are recruited into a single juvenile stage,  $\mathbf{F}$  is of rank one. That is,  $\mathbf{F}$  will have nonzero entries only in a single row or column. As a result, although calculating  $\lambda$  involves an  $N$ th-order polynomial, calculating  $R_0$  often involves a first-order polynomial (de-Camino-Beck and Lewis 2007; Rueffler and Metz 2013). This can allow for intuitive insight through a closed-form, analytical expression for  $R_0$ , expressed as the sum of contributions from different reproduction pathways in the life cycle (de-Camino-Beck and Lewis 2007). The possibility for similar insight in the context of spatial spread is tantalizing.

## Models

### *The Next-Generation Operator*

To model generational spread, we define a next-generation operator,  $\mathcal{L}_G$ , that describes change in population density across space from one generation to the next. By reworking the standard linearized IDE model of spread (1), we must keep track of all individuals produced by a given generation as it matures, spreads through space, and eventually dies (fig. 1). In defining  $\mathcal{L}_G$ , we retain assumptions about spatial homogeneity and density independence at the advancing invasion front (Neubert and Caswell 2000).

First, we rewrite the linearized IDE (1), decomposing  $\mathbf{A}$  to define fecundity and transition operators ( $\mathcal{L}_F$  and  $\mathcal{L}_T$ , respectively):

$$\begin{aligned} \mathbf{n}(x, t+1) &= \int_{-\infty}^{\infty} [\mathbf{K}(x-y) \circ (\mathbf{F} + \mathbf{T})] \mathbf{n}(y, t) dy \\ &= \underbrace{\int_{-\infty}^{\infty} [\mathbf{K}_F(x-y) \circ \mathbf{F}] \mathbf{n}(y, t) dy}_{\mathcal{L}_F \mathbf{n}(x, t)} \\ &\quad + \underbrace{\int_{-\infty}^{\infty} [\mathbf{K}_T(x-y) \circ \mathbf{T}] \mathbf{n}(y, t) dy}_{\mathcal{L}_T \mathbf{n}(x, t)}, \end{aligned} \quad (5)$$

where  $\mathbf{K}_F(x-y)$  and  $\mathbf{K}_T(x-y)$  are matrices of dispersal kernels associated with reproduction and transition, respectively. Expression (5) partitions population change into contributions from reproduction and associated dispersal ( $\mathcal{L}_F$ ) and contributions from development, survival, and associated dispersal ( $\mathcal{L}_T$ ).

Applied to the vector,  $\mathbf{u}(x, g)$ , of stage-specific densities that make up the population in generation  $g$ , the next-

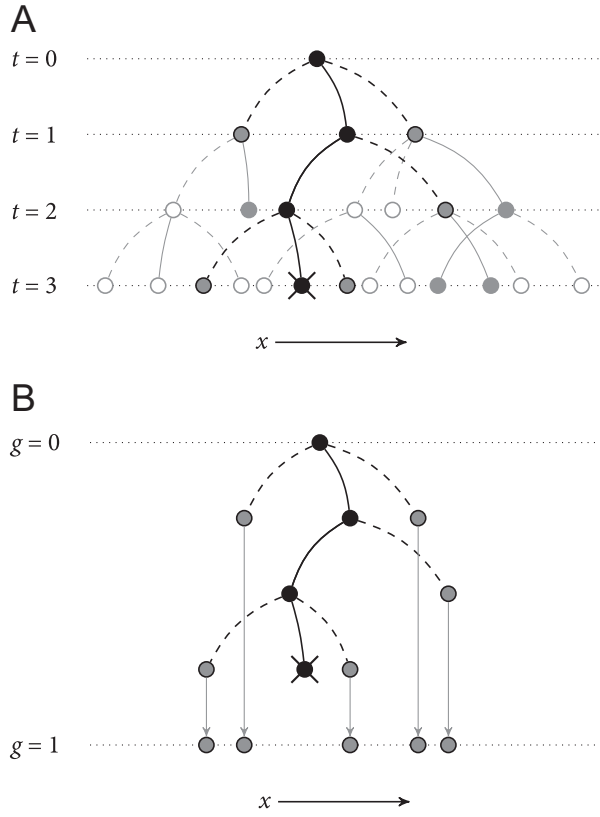


**Figure 1:** Diagram of annual spread (A) and resultant generational spread (B). Individual  $I$  (black circle) seeds generation  $g = 0$  at time  $t = 0$ , transitioning and moving (solid lines) in each time step, until its death at  $t = 3$ .  $I$  produces offspring (dashed lines, gray circles) that themselves transition, move, and produce offspring (white circles). The locations of  $I$ 's offspring, when initially produced, make up the spatial distribution of generation  $g = 1$ .

generation operator gives the densities of offspring in generation  $g + 1$ ,  $\mathbf{u}(x, g + 1)$ , produced as the individuals in generation  $g$  transition through time, reproducing and dispersing according to their life-history stage in each time step (fig. 1):

$$\begin{aligned} \mathbf{u}(x, g + 1) &= \mathcal{L}_G \mathbf{u}(x, g) \\ &= \mathcal{L}_F \mathbf{u}(x, g) + \mathcal{L}_F \mathcal{L}_T \mathbf{u}(x, g) + \mathcal{L}_F \mathcal{L}_T \mathcal{L}_T \mathbf{u}(x, g) + \dots \\ &= \mathcal{L}_F [\mathbf{I} + \mathcal{L}_T + \mathcal{L}_T^2 + \dots] \mathbf{u}(x, g). \end{aligned} \quad (6)$$

Note here that  $\mathbf{u}(x, g)$  is associated with a single generation,  $g$ , and not a single time step,  $t$ . Just as in human populations, multiple generations can be present at any given time, and the life spans of two individuals in the same generation need not overlap.

#### Generational Spreading Speed

We seek a spreading speed associated with the generation-by-generation dynamics described by equation (6). Similar

to analyses of standard annual invasion (Kot et al. 1996; Neubert and Caswell 2000), we look for limiting exponential-form solutions that progress a distance of  $c_G$  each generation:

$$\mathbf{u}(x, g) = \mathbf{w}_G e^{-s_G(x - c_G g)}, \quad (7)$$

where  $\mathbf{w}_G$  describes the relative abundances of stage classes in a traveling wave and  $s_G$  describes the shape of the wave.

In “Derivation of Generational Spreading Speed” in the appendix, we derive the generational spreading speed for a population, initially introduced locally:

$$c_G^* = \min_{s_G \in \Omega_G} \left[ \frac{1}{s_G} \ln(\rho_1[\mathbf{H}_G(s_G)]) \right], \quad (8)$$

where matrix  $\mathbf{H}_G(s_G)$  is  $\mathbf{H}_F(s_G)[\mathbf{I} - \mathbf{H}_T(s_G)]^{-1} = [\mathbf{M}_F(s_G) \circ \mathbf{F}] [\mathbf{I} - \mathbf{M}_T(s_G) \circ \mathbf{T}]^{-1}$  and  $\mathbf{M}_F(s_G)$  and  $\mathbf{M}_T(s_G)$  are the matrices of moment-generating functions for the reproduction- and transition-specific dispersal kernels, respectively.  $\Omega_G$  is the domain of existence for the wave-speed function being minimized. We denote the wave shape at which  $c_G^*$  is attained by  $s_G^*$ .

$\mathbf{H}_G(s_G)$  is the invasion analog of the next-generation matrix,  $\mathbf{Q}$ , incorporating information about both demography and dispersal, and equation (8) yields an asymptotic generational rate, similar to  $R_0$ . Here, as for  $R_0$  calculations, the result pertains to dynamics at low density, which are well described on an annual timescale by the linearized model (5). We go on to show how our generational measure relates to these linearized dynamics and thereby how it relates to the dynamics of the relevant nonlinear (“true”) model (Lui 1989a).

Note that  $\Omega_G$ , the domain over which we must minimize in (8), is more restricted than  $\Omega$  in (3). In  $\Omega_G$ , not only must  $\mathbf{M}(s_G)$  and  $1/s_G$  exist, but  $\rho_1[\mathbf{H}_T(s_G)]$  must be  $< 1$ , so that  $[\mathbf{I} - \mathbf{H}_T(s_G)]^{-1}$  exists. This extra transition-related condition means that generational spread occurs over a more restricted range of density profiles than annual spread. We interpret this as indication that steeper invasion fronts effectively collapse when individuals disperse as they survive and mature. Repeated dispersal over the course of a lifetime is compounded, and a given annual dispersal pattern can lead to a considerably more diffuse pattern of lifetime dispersal.

Recall that  $\mathbf{u}(x, g)$  is not associated with any specific time step, and single generations can be spread over long time periods. In the mathematical idealization, most stage-specific mortality comprises exponential decay, and single generations are spread across an infinitely long time window. While this would not be the case in real populations, in which individuals are discrete units that must die eventually, it would not in general be possible to measure gen-

erational spreading speed or the shape of a generational spreading front.

### *Conditions for Spread*

In the context of demography, the inequalities (4) reveal that the net reproductive number,  $R_0$ , and the population growth rate,  $\lambda$ , are both indicators of population growth or decline (Cushing and Yicang 1994; Li and Schneider 2002). Our analysis reveals a similar relationship between the generational spreading speed,  $c_G^*$ , and the annual spreading speed,  $c^*$ . In “Invasion Criteria” in the appendix, we show that the sign of  $c_G^*$  matches the sign of  $c^*$ . As a result, knowing whether a species’ generational spreading speed is greater than 0 is enough to know whether the population will, in theory, spread.

Although we show that population spread proceeds at least as far in a generation as it does in a year (i.e., that  $|c_G^*| \geq |c^*|$ ), we note that the magnitude of changes in generational wave speed do not necessarily predict the magnitude of changes in standard wave speed. The critical point is that  $c_G^*$  and  $c^*$  share the same sign and are, therefore, equally good—or equally bad—theoretical indicators of whether a population will spread in space.

### *Comparisons of Generation Time*

In demography, generation time,  $T_G$ , is often defined as the time required for a population at stable stage distribution to grow by a factor of  $R_0$ . That is,

$$\lambda^{T_G} = R_0 \iff T_G = \frac{\ln(R_0)}{\ln(\lambda)} = \frac{\ln(\rho_1[\mathbf{Q}])}{\ln(\rho_1[\mathbf{A}])} \quad (9)$$

(Caswell 2001; de-Camino-Beck and Lewis 2008).

At the leading edge of an invasion, there are additional relevant timescales we could calculate. If we choose a location near the invasion front, the apparent population growth rate (incorporating both local demography and density increases due to dispersal) is  $n_i(x, t+1)/[n_i(x, t)]$  for any  $i$ , assuming the invasion wave has attained a stable stage distribution. By (2),

$$\frac{n_i(x, t+1)}{n_i(x, t)} = \frac{e^{-s^*(x - c^*[t+1])}}{e^{-s^*(x - c^*t)}} = e^{s^*c^*}. \quad (10)$$

Similarly, the apparent per-generation population growth rate is  $e^{s_G^*c_G^*}$ . Following the argument of (9) and substituting (3) and (8), the apparent generation time at our location near the invasion front is

$$T_x = \frac{\ln(e^{s_G^*c_G^*})}{\ln(e^{s^*c^*})} = \frac{s_G^*c_G^*}{s^*c^*} = \frac{\ln(\rho_1[\mathbf{H}_G(s_G^*)])}{\ln(\rho_1[\mathbf{H}(s^*)])}. \quad (11)$$

For an observer at a fixed location near the leading edge of the invasion front, this is the time it takes the invading population to increase by as much as it would from one generation to the next at the same location. This differs from the standard concept of generation time in that the population “growth” observed near the front is actually due to a combination of population growth and population dispersal at a given location rather than growth alone across the whole population.

Alternatively, we could consider generation spreading time—the time it takes for the population to spread as far as it would over the course of one generation:

$$T_c = \frac{c_G^*}{c^*} = \frac{s^* \ln(\rho_1[\mathbf{H}_G(s_G^*)])}{s_G^* \ln(\rho_1[\mathbf{H}(s^*)])} = \frac{s^*}{s_G^*} T_x. \quad (12)$$

Instead of considering “growth” at a fixed location, (12) considers the generation-time analog relevant to spread. Here, spread occurs linearly, as opposed to geometrically in the case of increases in population density. Because of the exponential shape of the linearized invasion wave, however,  $T_x$  and  $T_c$  have very similar forms.

## Calculations

### *Order of the Characteristic Equation*

We seek to use the concept of generational spreading speed to gain insight into the process of invasion and ways that it might stall. As for  $\lambda$ , we must often calculate  $\rho_1[\mathbf{H}(s)]$  numerically, since the characteristic equation of  $\mathbf{H}(s)$  is an  $N$ th-order polynomial. Because of its direct dependence on  $\mathbf{F}$ , however,  $\mathbf{H}_G(s_G)$  will often be of rank one, with a first-order characteristic equation (de-Camino-Beck and Lewis 2007; Rueffler and Metz 2013). Thus, a component of  $c_G^*$  can often be expressed as a simple mathematical equation.

De Camino-Beck and Lewis (2007) developed a graph-reduction method for algebraically calculating  $R_0$ . We have adapted their techniques to calculate  $\rho_1[\mathbf{H}_G(s_G)]$ , which we call  $R_c(s_G)$ , when  $\mathbf{H}_G(s_G)$  is of rank one (see “Graph-Reduction Calculations” in the appendix). Multiple demographic scenarios are compatible with this approach, but in broad terms all reproductive pathways must pass through a single life-history stage (see Rueffler and Metz 2013 for technical details).

### *Simplification and Approximation*

In “Derivation of Generational Spreading Speed” in the appendix, we analyze the case in which dispersal is associated solely with reproduction, as for many plants and sedentary aquatic organisms with a planktonic larval phase,

and dispersal patterns are consistent across reproductive stages, as might be expected for seeds or waterborne larvae. The condition that juvenile dispersal does not depend on the parent stage would be violated, for example, if seeds from large trees disperse farther than seeds from small trees. The generational spreading speed becomes

$$c_G^* = \min_{s_G \in \Omega_G} \left( \frac{1}{s_G} \ln[m(s_G)R_0] \right). \quad (13)$$

This is the same form as for unstructured populations, in which  $R_0 \equiv \lambda$  when generations do not overlap (Kot et al. 1996; Lutscher 2007). This arises because dispersal occurs only once in such an organism's life history:  $R_0$  indicates how many offspring each individual produces throughout its lifetime, and  $m(s_G)$  provides information about the single spatial transition those offspring make. The associated annual case is little different, except that the relevant offspring are produced in a single year.

If newly produced individuals also disperse according to a normal distribution with mean  $\mu$  and standard deviation  $\sigma$ , then

$$c_G^* = \mu + \sigma \sqrt{2 \ln(R_0)} \quad (14)$$

(see "Derivation of Generational Spreading Speed" in the appendix). Here, the generational spreading speed (14) matches the conventional spreading speed for the case of growth and normal (Gaussian) dispersal in an unstructured population (Kot et al. 1996) except that the spreading speed will be in units of distance per generation. Commonly  $\mu$  may be 0, but  $\mu$  will be nonzero in the cases of biased dispersal due to current, wind, or animal migration.

Without the assumption of Gaussian dispersal, we cannot solve for a general closed-form asymptotic spreading speed. Instead, if individuals disperse symmetrically, we can apply an approximation (Lutscher 2007):

$$\tilde{c}_G^* = 2\sigma \sqrt{\frac{\ln(R_0)}{2}} + \frac{\sigma}{3} \left( \sqrt{\frac{\ln(R_0)}{2}} \right)^3 \gamma, \quad (15)$$

where  $\sigma$  is the standard deviation of the symmetric dispersal kernel and  $\gamma$  is the excess kurtosis of the dispersal kernel relative to the normal distribution, so that  $\gamma = \mu_4/\sigma^4 - 3$ , where  $\mu_4$  is the fourth central moment (kurtosis) of the dispersal kernel (see "Derivation of Generational Spreading Speed" in the appendix; Lutscher 2007).

## Examples

Concepts related to generational spreading speed allow for a deeper understanding of the spatiodemographic process of population spread but also provide several practical benefits for empiricists and managers (table 1). Because generational and annual spreading speeds coincide at 0 (stalled spread), the simpler calculations associated with generational spread can be used to explore this critical threshold. In addition, using graph reduction to calculate generational spreading speed lends itself to intuitive interpretation of demographic events influencing spreading rate. This can complement elasticity analysis of annual spreading speed, much as graph reduction can be used to gain insight into demographic factors affecting generational population growth (de-Camino-Beck and Lewis 2007).

In this section, we offer three examples taken from the literature that illustrate applications of generational spreading speed. The first considers a stalled invasion of green crabs in Nova Scotia, which yields an analytical expression from which we estimate larval recruitment—an otherwise difficult-to-estimate parameter. The second example, which considers California sea otters, illustrates important differences between standard and generational spreading speeds and highlights another case in which invasion can stall even when population growth is positive. In the final example, we reanalyze the classic case of teasel invasion in the context of generational spread and explore how the use of

**Table 1:** Measures of population growth and spread for discrete-time models incorporating an  $N$ -stage life history

Quantity	Calculation	Application
$\lambda$ : Annual rate of population increase	Solution to $N$ th-order polynomial	Clear interpretation as rate of population increase but often must be computed numerically
$R_0$ : Generational rate of population increase	Typically the solution to first-order polynomial	Equivalent to $\lambda$ as indicator of population growth or decline and often has closed analytic form, facilitating interpretation of life-history parameter influences
$c^*$ : Annual spreading speed	Involves solution of $N$ th-order polynomial	Clear interpretation as rate of population spread but usually must be computed numerically
$c_G^*$ : Generational spreading speed	Typically involves solution of first-order polynomial	Equivalent to $c^*$ as indicator of population spread or stall, can be easier to interpret influences of life-history parameters, closed analytic form in the case of Gaussian dispersal

Note: Rows 1 and 2 relate to population-projection matrices; rows 3 and 4 relate to integrodifference equations.

graph-reduction techniques can yield insight into factors affecting invasion.

While our approach provides a powerful new analytical tool, we do not claim to treat any one of our example systems fully. Such comprehensive analyses—for example, incorporating model and parameter uncertainty—are beyond the scope of our present discussion. Instead, we provide the following as pedagogical examples, illustrating where the concepts of generational spreading speed could provide useful insight.

#### *European Green Crab*

The European green crab, *Carcinus maenas*, has invaded coastlines around the globe from its native range in the northeast Atlantic (Audet et al. 2003). On the east coast of North America, *C. maenas* had arrived in New York by 1817, slowly spreading north until it began a more rapid range expansion around the Gulf of Maine in the first half of the twentieth century (Audet et al. 2003). Green crabs had reached Halifax, Nova Scotia, by 1964, but their northern expansion seemed to stall there, likely due to low water temperatures (Berrill 1982; Audet et al. 2003). Here, we use the concept of generational wave speed to explore the stall of the original *C. maenas* invasion near Halifax and, on the basis of previously published survival and dispersal estimates, produce an analytical estimate for a notoriously difficult-to-estimate parameter—per-adult larval recruitment. Kanary et al. (2014) have presented an alternative IDE model that considers green crab competition; however, we use a simplified model for the purposes of illustration.

In the northwest Atlantic, crabs mature at approximately 2.5 years and live for approximately 5.5 years (Berrill 1982). Per capita recruitment of juveniles is unknown. This gives the following transition and fecundity matrices:

$$\mathbf{F} = \begin{bmatrix} 0 & f \\ 0 & 0 \end{bmatrix} \text{ and } \mathbf{T} = \begin{bmatrix} 3/11 & 0 \\ 6/11 & 9/11 \end{bmatrix}. \quad (16)$$

Pringle et al. (2011) estimated larval dispersal to be normally distributed with a mean of  $\mu = -67$  km and a standard deviation of  $\sigma = 234$  km. Mean dispersal is negative due to the southern direction of the prevailing current, opposite to the northern direction of stalled invasion that we consider as the positive  $x$ -direction. Relative to larvae, we can assume that juvenile and adult crabs are fixed, so the asymptotic generational wave speed will be given by (14):  $c_G^* = \mu + \sigma[2 \ln(R_0)]^{1/2}$ .

Graph reduction gives  $R_0 = 33/8f$ , and substitution of  $R_0$ ,  $\mu$ , and  $\sigma$  into (14) gives the speed of the northward invasion:  $c_G^* = -67 + 234[2 \ln(33/8f)]^{1/2}$  (see “Example Details” in the appendix). Setting  $c_G^*$  equal to 0 (since we are considering a stalled invasion) and solving for  $f$  reveals that

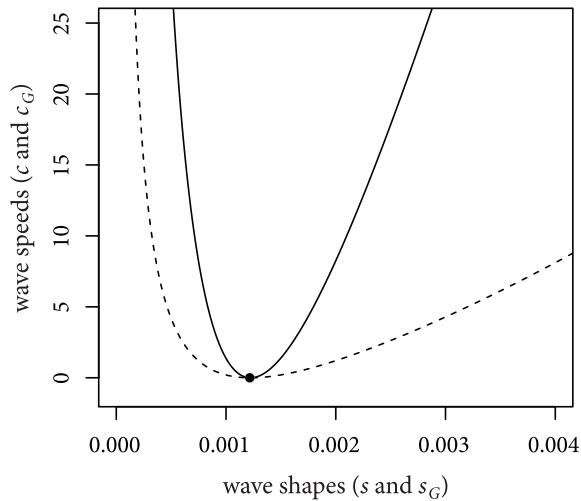


**Figure 2:** Standard (dashed; km/year) and generational (solid; km/generation) invasion speeds as a function of respective wave shape for the European green crab, *Carcinus maenas*. The shared critical value (black circle) portrays stalled northward invasion near Halifax, Nova Scotia, after 1964.

each crab would have to produce fewer than approximately 0.253 successful recruits per year, or about one recruit per female every other year, to halt invasion under the conditions described. Note that this level of fecundity corresponds to  $R_0 \approx 1.04$ , so the population would grow in the absence of spread and also spread northward in the absence of a southerly current.

Here, we could have used standard spreading-speed calculations, applying equation (3) to calculate the annual invasion speed,  $c^*$ . A partial analytical solution would be possible:  $\rho_1[\mathbf{H}] = 6/11 + ([3/11]^2 + 6/11f \exp[(117/2)^2s - 67]s)^{1/2}$ . However, we would be left with a numerical minimization:  $c^* = \min_{s \geq 0} [1/s \ln(\rho_1[\mathbf{H}(s)])]$ . Although this would yield the same answer, such a solution would be much less satisfying. Note that  $c^* = c_G^*$  for the stalled northward invasion (fig. 2) but that annual and generational spreading speed will not be equal in general.

#### *California Sea Otter*

California sea otters were hunted nearly to extinction in the early 1900s, but a small population was protected in 1914, and the species has since recolonized some of its historical range (Lubina and Levin 1988; Tinker et al. 2008). Several authors have used IDEs to model sea otters’ recolonization of the California coastline (Krkosk et al. 2007; Tinker et al. 2008; Smith et al. 2009). Unlike the species in our other examples, mature otters are thought to disperse (Krkosk et al. 2007), and we use the simplest existing integrodifference model (Krkosk et al. 2007) to illustrate

how later-life dispersal affects generational spread. We also illustrate how spreading speeds relate to demographic measures of population growth,  $\lambda$  and  $R_0$ , and further explore how dispersal and demography can interact to halt spread even for a growing population.

Sea otters breed once a year and progress through distinct life stages (pup, juvenile, adult). Estimates for otter survival and reproduction yield a relatively simple population projection matrix,  $\mathbf{A} = \mathbf{F} + \mathbf{T}$ , with

$$\mathbf{F} = \begin{bmatrix} 0 & 0 & 0.45 \\ 0 & 0 & 0 \\ 0 & 0 & 0 \end{bmatrix} \text{ and } \mathbf{T} = \begin{bmatrix} 0 & 0 & 0 \\ 0.6 & 0.631 & 0 \\ 0 & 0.269 & 0.9 \end{bmatrix} \quad (17)$$

(compiled in Krkošek et al. 2007).

We assume that juvenile and adult sea otters disperse according to a Laplace kernel,  $(2\alpha)^{-1} \exp(-|x - y|/\alpha)$ , with  $\alpha = 5.19$  km—the best exponentially bounded kernel fit to dispersal-distance data by Krkošek et al. (2007). The Laplace kernel predicts constant spreading speed, consistent with observed bouts of constant-speed recolonization (Lubina and Levin 1988). To complete the matrices  $\mathbf{H}_F(s_G)$  and  $\mathbf{H}_T(s_G)$ , we need to know the moment-generating function for the Laplace kernel, given by  $[1 - (5.19s_G)^2]^{-1}$ . Pups do not disperse, which is represented mathematically as a dispersal kernel called the Dirac delta function,  $\delta(x - y)$ , concentrated at  $y$ , for which the moment-generating function is simply 1 (Krkošek et al. 2007), so that

$$\mathbf{H}_F(s_G) = \begin{bmatrix} 0 & 0 & \frac{0.45}{1 - (5.19s_G)^2} \\ 0 & 0 & 0 \\ 0 & 0 & 0 \end{bmatrix} \quad (18)$$

and

$$\mathbf{H}_T(s_G) = \begin{bmatrix} 0 & 0 & 0 \\ 0.6 & \frac{0.631}{1 - (5.19s_G)^2} & 0 \\ 0 & \frac{0.269}{1 - (5.19s_G)^2} & \frac{0.9}{1 - (5.19s_G)^2} \end{bmatrix}.$$

We must be careful to consider the constraint imposed on  $s_G$  by the condition  $\rho_1[\mathbf{H}_T(s_G)] < 1$ . Recall that this condition restricts the range of exponential generational wave shapes the spreading population can attain as a result of dispersal during maturation and survival. Solving  $\rho_1[\mathbf{H}_T(s_G)] < 1$  algebraically (see “Example Details” in the appendix), we get an upper bound on  $s_G$  of approximately  $0.0609 \text{ km}^{-1}$ , less than the  $(5.19 \text{ km})^{-1} = 0.193 \text{ km}^{-1}$  upper bound imposed by the existence of the moment-generating func-

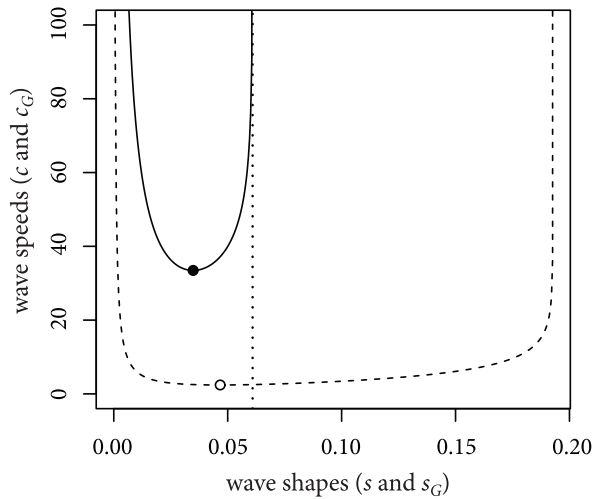


**Figure 3:** Standard (dashed; km/year) and generational (solid; km/generation) recolonization speeds as a function of respective wave shape for the California sea otter, *Enhydra lutris nereis*. The vertical dotted line shows the upper bound on the domain of the generational wave-speed function. Circles show the asymptotic wave speed and wave shape for generational (filled) and annual (open) spread.

tions. Here,  $c_G(s_G)$  has a more restricted wave-shape domain than  $c(s)$  (fig. 3). Were we to ignore the more restrictive upper bound, we could get results that indicate incorrect, excessively fast generational spread, especially if we were to perform the minimization in (8) numerically.

Although fairly simple, the sea otter integrodifference model did a reasonable job of capturing recolonization progress in California until at least the mid-1980s (Krkošek et al. 2007). In recent years, however, the northward sea otter recolonization has stalled just south of San Francisco (T. Tinker, personal communication). The generational spreading speed can be used to consider the potential role played by two factors. First, otter dispersal may be biased southward due to offshore currents (Lubina and Levin 1988; Smith et al. 2009), and second, otters’ survival appears to decline toward the north of their range (Tinker et al. 2006).

To account for south-biased dispersal, we replace the juvenile and adult dispersal kernel with a biased Laplace kernel that depends on parameter  $\vartheta$ , the proportion of individuals dispersing south, and recovers the original unbiased kernel when  $\vartheta = 0.5$  (see “Example Details” in the appendix). To consider a range of possible survival values beyond the northern recolonization boundary, we introduce scaling parameter  $\varphi$  and replace the original sea otter transition matrix with a scaled version,  $\varphi\mathbf{T}$ .

Using (3) and (A21), we numerically solved for annual and generational spreading speeds across a range of  $\vartheta$  and  $\varphi$  values to explore conditions that could have halted the northern advance of the sea otter population (fig. 4). As we have proven (see “Invasion Criteria” in the appendix),

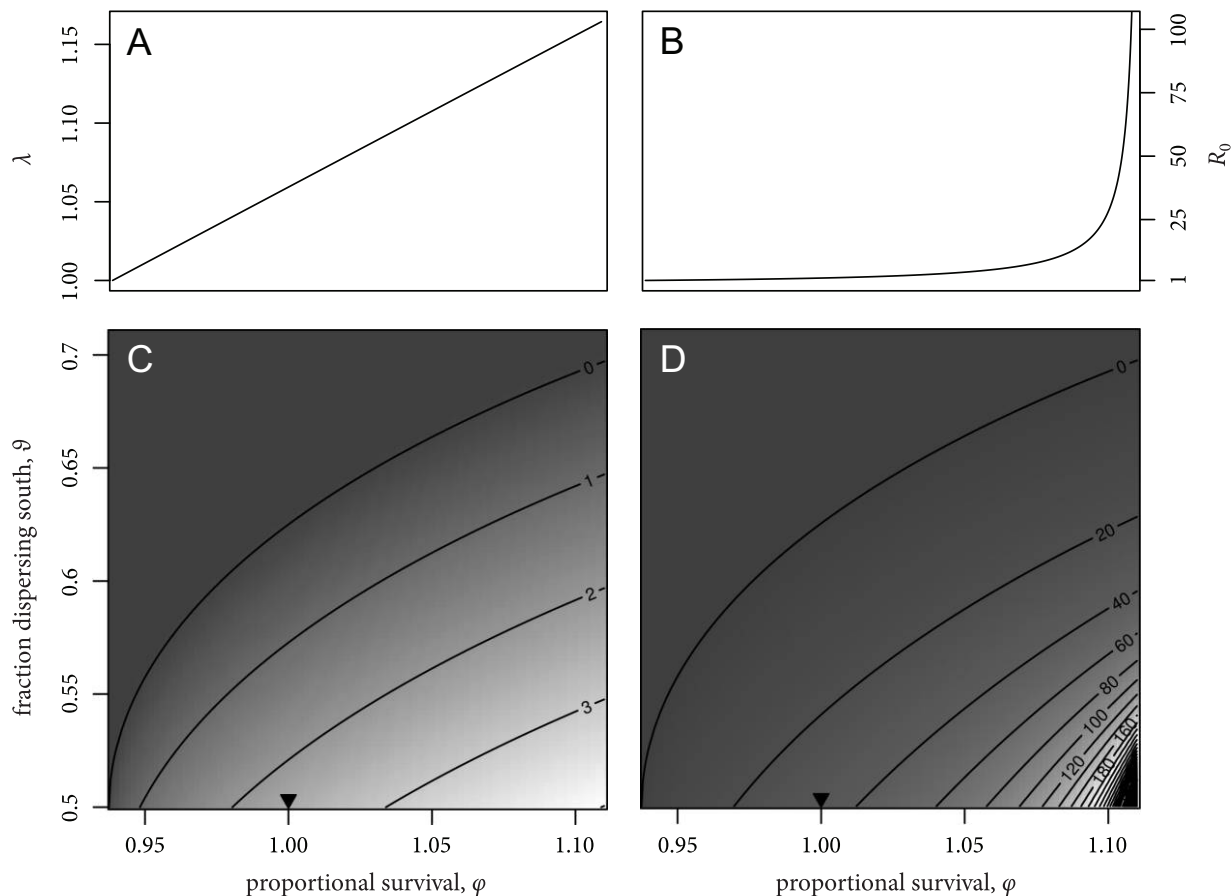


**Figure 4:** Rates of growth and spatial spread for the California sea otter, *Enhydra lutris nereis*, in an environment with south-biased dispersal. A and B show the annual population growth rate ( $\lambda$ ) and the generational population growth rate ( $R_0$ ), respectively, for a range of survival-scaling factors,  $\varphi$ . Higher  $\varphi$  yields proportionally higher survival across age classes. C and D show annual spreading speed ( $c^*$ ) and generational spreading speed ( $c_G^*$ ), respectively, for combinations of  $\varphi$  and the fraction of individuals dispersing south,  $\vartheta$ . In C and D, the upper-left dark-gray region indicates a lack of northward range expansion (negative speeds not shown), while the region to the lower right of the 0-contour line indicates recolonization; arrows correspond to parameter values from Krkošek et al. (2007). Note that as  $\varphi$  approaches 1/0.9, annual mortality unrealistically declines to 0; associated values are for illustration only.

both measures of spreading speed predict stalled northern recolonization in the same parameter region, and  $c_G^* > c^*$  where spreading speed is positive. Note that recolonization could have stalled, even for a growing population ( $R_0 > 1$ ), if dispersal were biased. Relative to the parameter values used by Krkošek et al. (2007), approximately 65% of adult and juvenile otters would have had to disperse south or otter survival rates would have had to decline to approximately 93.7% of their observed values to stop northward spread.

#### Wild Teasel

Wild teasel is a flowering plant, native to Eurasia, that now grows as a weed along roadsides and in fields in southeastern Canada and the northern United States (Werner

1975a). Increasingly problematic as an invasive species, teasel has garnered attention as a candidate for biological control (Rector et al. 2006). Neubert and Caswell (2000) considered teasel in their development of invasion speed for stage-structured populations, and we consider it again here. We show how graph reduction and approximation of generational spreading speed can yield insight into the process of invasion and help identify targets for biological control.

Teasel seeds can remain dormant for a number of years, progress through several rosette stages after germination, and finally grow a tall (0.5–2.5-m) stalk that flowers and drops seeds before the plant dies (Werner 1975a, 1975b). Werner and Caswell (1977; Caswell 2001) studied the demography of teasel in eight experimental fields, measuring and modeling demographic rates for six life-history stages. Annual demographic transitions in the field with the high-

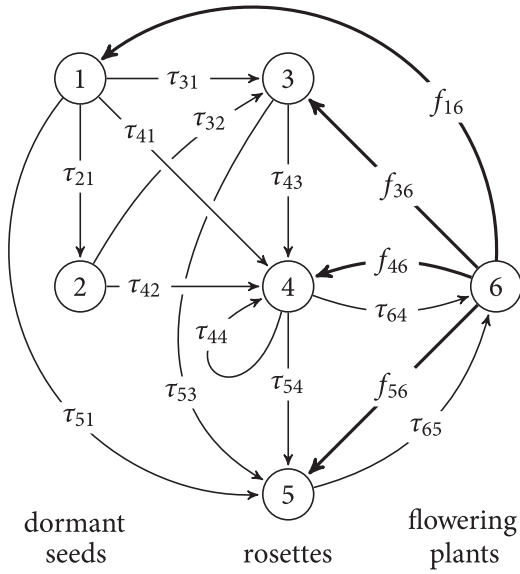


**Figure 5:** Life-cycle graph for teasel, *Dipsacus fullonum*. The  $\tau_{ij}$ 's represent survival and maturation transitions between life stages, and the  $f_{ij}$ 's represent stage-specific fecundities.

est asymptotic population growth rate (fig. 5; Werner and Caswell 1977; Caswell 2001) are summarized in the following fecundity and survival matrices:

$$\mathbf{F} = \begin{bmatrix} 0 & 0 & 0 & 0 & 0 & 402.59 \\ 0 & 0 & 0 & 0 & 0 & 0 \\ 0 & 0 & 0 & 0 & 0 & 8.255 \\ 0 & 0 & 0 & 0 & 0 & 69.215 \\ 0 & 0 & 0 & 0 & 0 & 3.810 \\ 0 & 0 & 0 & 0 & 0 & 0 \end{bmatrix}$$

and

$$\mathbf{T} = \begin{bmatrix} 0 & 0 & 0 & 0 & 0 & 0 \\ 0.974 & 0 & 0 & 0 & 0 & 0 \\ 0.017 & 0.011 & 0 & 0 & 0 & 0 \\ 0.004 & 0.002 & 0.077 & 0.212 & 0 & 0 \\ 0.003 & 0 & 0.038 & 0.281 & 0 & 0 \\ 0 & 0 & 0 & 0.063 & 1.000 & 0 \end{bmatrix}. \quad (19)$$

Taking demographic rates in this field as representative of low-density conditions and modeling one-dimensional seed spread using a symmetric Laplace distribution,  $k_{16}(x - y) = (2\alpha)^{-1} \exp(-|x - y|/\alpha)$ , with mean dispersal distance  $\alpha = 0.257$  m (Werner 1975b), Neubert and Caswell (2000) calculated teasel's asymptotic spreading speed as 0.564 m/year, with a wave shape of  $3.20 \text{ m}^{-1}$ .

In line with previous analysis (Neubert and Caswell 2000), we consider the idealized case of teasel dispersing in a one-dimensional environment. This would be appropri-

ate for a population advancing along a roadside or stream bank, for example, but important differences arise in truly two-dimensional environments, such as a field (Lewis et al. 2006; de-Camino-Beck and Lewis 2009). In any case, teasel's spread across large spatial scales may rely on long-distance dispersal mechanisms, such as transport along river systems (Neubert and Caswell 2000).

Although there is an algebraic expression for teasel's  $R_c(s_G)$ , we must calculate the critical wave speed numerically. Applying graph reduction (see "Graph-Reduction Calculations" in the appendix), we get

$$R_c(s_G) = m(s_G)R_0, \quad (20)$$

where

$$R_0 = \left[ \left( \frac{(\tau_{64} + \tau_{65}\tau_{54})[\tau_{41} + \tau_{42}\tau_{21} + \tau_{43}(\tau_{31} + \tau_{32}\tau_{21})]}{1 - \tau_{44}} \right. \right. \\ \left. \left. + \tau_{65}[\tau_{51} + \tau_{53}(\tau_{31} + \tau_{32}\tau_{21})] \right) f_{16} \right. \\ \left. + \left( \frac{(\tau_{64} + \tau_{65}\tau_{54})\tau_{43}}{1 - \tau_{44}} + \tau_{65}\tau_{53} \right) f_{36} \right. \\ \left. + \frac{(\tau_{64} + \tau_{65}\tau_{54})}{1 - \tau_{44}} f_{46} + \tau_{65}f_{56} \right]; \quad (21)$$

the  $f_{ij}$ 's are entries of  $\mathbf{F}$ , the  $\tau_{ij}$ 's are entries of  $\mathbf{T}$ , and  $m(s_G)$  is the moment-generating function for the Laplace distribution:  $(1 - \alpha^2 s_G^2)^{-1}$ , defined for  $s_G < 1/\alpha = 3.89 \text{ m}^{-1}$ . Substituting the transition and fecundity values from (19), equation (21) gives  $R_0 = 37.7$ . Incorporating  $R_c(s_G)$  into

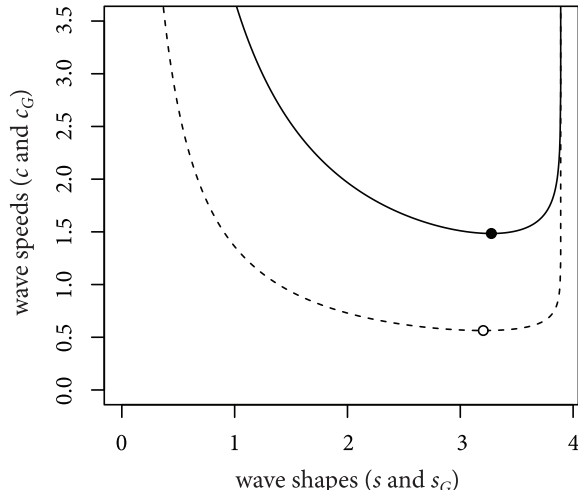


**Figure 6:** Standard (dashed; m/year) and generational (solid; m/generation) spreading speeds as a function of respective wave shape for teasel, *Dipsacus fullonum*. Circles show the asymptotic wave speed and wave shape for generational (closed) and annual (open) spread.

equation (8) and numerically solving for the minimum (fig. 6), we get  $c_G^* = 1.48$  m/generation at  $s_G^* = 3.28$  m<sup>-1</sup>.

Comparing demographic rates and invasion speeds, we can calculate the different measures of generation time (see “Comparisons of Generation Time”). Standard generation time,  $T_G$ , is  $\ln(R_0)/\ln(\lambda) = 2.72$ . Apparent generation time for a focal location near the invasion front,  $T_s$ , is  $s_G^* c_G^*/(s^* c^*) = 2.69$ . Generation spreading time,  $T_c$ , is  $c_G^*/c^* = 2.63$ . That is, it would take 2.72 years for a small teasel population to grow overall by the same amount as it would grow in a single generation, 2.69 years for population density at the leading edge of an invasion to increase by the same amount as it would in a single generation, and 2.63 years for the invasion to advance as far as it would in a single generation. These are mathematical quantities, and given that growth and spread occur in discrete steps, none of these events would have occurred after 2 years, but all would have occurred by 3 years.

Although dispersal according to a Laplace distribution does not yield a simple closed-form estimate for asymptotic spreading speed, we can use moment-based approximation (15). The second moment and excess kurtosis of the Laplace distribution are  $\sigma^2 = 2\alpha^2$  and  $\gamma = 3$ , respectively. This yields a generational spreading-speed estimate of

$$\tilde{c}_G^* = 0.514\sqrt{\ln(R_0)} + 0.1285\left(\sqrt{\ln(R_0)}\right)^3, \quad (22)$$

which equals 1.87 m/generation, for teasel. As teasel’s transition and fecundity rates change, influencing  $R_0$ ,  $c_G^*$  increases not only with the square root of  $\ln(R_0)$ , as when dispersal is Gaussian, but also approximately with the cube of the square root of  $\ln(R_0)$ .

Examining the influence of reproductive pathways on  $R_0$  (de-Camino-Beck and Lewis 2007), we can gain insight, similar to that from  $c^*$ -elasticity calculations, into life-history factors that affect spreading speed. Teasel’s annual invasion speed is most elastic to changes in transition through, and reproduction into, advanced rosette stages ( $\tau_{54}$ ,  $\tau_{64}$ ,  $\tau_{65}$ ,  $f_{46}$ , and  $f_{56}$ ; Neubert and Caswell 2000). From (21), we would draw similar conclusions. At observed transition and fecundity values, the first two reproductive pathways in teasel’s  $R_0$  expression account for very little of the observed generational increase—8% and 2%, split among numerous subpathways—so early-stage transition and fecundity terms that appear only in those pathways will have relatively little influence on  $R_0$ . On the other hand, the latter two reproductive pathways, in which the late-stage terms are clustered, account for the vast majority of the observed generational increase—80% and 10%, consolidated in few subpathways. Reexamining teasel’s life-cycle graph and projection-matrix components (fig. 5; eq. [19]), we see that all individuals must pass through one of the latter rosette stages to reproduce, and although flowers produce

a large number of dormant seeds, those seeds rarely germinate to produce viable plants.

Rector et al. (2006) identified candidate biological control agents for teasel, indicating rosette stages as primary targets for control and seeds and flowers as secondary targets (Rector et al. 2006). Our analysis, and that of Neubert and Caswell (2000), corroborates these conclusions. Control measures that hinder rosette maturation or that reduce seed germination (not necessarily seed production overall) should affect  $R_0$  most, thereby driving generational spreading speed furthest toward 0.

## Discussion

We have shown how to calculate generational spreading speed, an  $R_0$ -like quantity for spatially expanding populations, thereby completing the set of four foundational quantities to describe the spatiotemporal dynamics of population growth and spread. Generational spreading speed,  $c_G^*$ , relates to annual spreading speed,  $c^*$  (Neubert and Caswell 2000), in the same way that the net reproductive number,  $R_0$ , relates to the annual population growth rate,  $\lambda$ . In addition,  $c_G^*$  relates to  $R_0$  in the same way that  $c^*$  relates to  $\lambda$ : each measure of spreading speed is the spatial analog of its purely demographic counterpart.

As a complement to standard spreading speed (Neubert and Caswell 2000), generational spreading speed offers a number of advantages. First, in many biologically relevant cases, it is possible to calculate an algebraic expression for  $c_G^*$ . This is because reproduction often occurs from or to a single life-history stage, and the next-generation matrix takes a simplified form (see “Order of the Characteristic Equation”; de-Camino-Beck and Lewis 2007; Rueffler and Metz 2013). In the case of Gaussian dispersal, this leads to an explicit analytic form for the generational spreading speed (see “Simplification and Approximation”). Second, even if we cannot generate an explicit expression for generational spreading speed, we can examine the influence on generational spreading speed of reproductive pathways, elucidated via graph reduction (de-Camino-Beck and Lewis 2007) or algebra (Rueffler and Metz 2013). This can yield insight into life-cycle events of particular importance for a species’ ability to spread. When dispersal is unbiased, there is potential for further insight through moment-based approximations of generational spreading speed (see “Simplification and Approximation”).

When dispersal is directionally biased, as for green crabs, numerical population growth does not guarantee spread or even persistence (Lutscher et al. 2010). Spread in the less common dispersal direction can be stopped even if a population continues to grow (figs. 2, 4). In such cases, generational spreading speed can help determine the invasion

potential of a species and assess the plausibility of proposed control measures. Because  $c^*$  and  $c_G^*$  have the same sign (see “Invasion Criteria” in the appendix), a positive generational invasion speed guarantees that a species has the potential to spread from one year to the next. Control measures that reduce  $c_G^*$  to 0 are those that will halt invasion. As  $c_G^*$  can be simpler to calculate than  $c^*$ , it presents an attractive option, and consideration of control measures as they affect reproductive loops associated with  $c_G^*$  could yield useful insights.

Although we have not dealt with the concept of uncertainty in parameter estimates, we could employ the techniques discussed above. Using an analytical (or partial analytical) form for the generational spreading speed, it may be possible to understand intuitively how parameter uncertainty translates into uncertainty in the spreading speed.

Calculation of generational spreading speed involves one important constraint that, although not complicated, is not a consideration for annual spreading speed. Dispersal associated with demographic transitions can constrain the “wave” shape of the exponential-form generational invasion front, since  $\rho_1[\mathbf{H}_T(s_G)]$  must be less than 1 (see “Generational Spreading Speed”). For example, sea otters disperse as juveniles and adults rather than during recruitment into the population. As a result, their generational wave shape is more constrained than their annual wave shape (fig. 3). Although we have a guarantee that generational and standard spreading speed provide the same information about whether (re)invasion will proceed (see Invasion Criteria” in the appendix), it is important to remember the  $\rho_1[\mathbf{H}_T(s_G)] < 1$  constraint when calculating generational spreading speed; failure could lead to nonsensical results, especially when generational spreading speed is calculated numerically for complex cases. Falsely identifying a generational spreading speed associated with a wave shape outside the allowable range could lead to incorrect inference about whether a population will spread.

Consideration of spatial spread complicates the calculation of generation time compared with the case of purely demographic population growth. Similarities between spatial and nonspatial cases, however, mean that  $T_{\text{ss}}$ , apparent generation time at a given location, bears a close resemblance to the purely demographic measure of generation time,  $T_G$ . Even  $T_{\text{ss}}$ , the version of generation time relating generational spread and annual spread—linear rather than geometric processes—takes a form similar to that of  $T_G$  because of the exponential shape of the limiting invasion front (7). In the case of teasel, the measures of generation time are relatively similar, but a naive stationary observer near the invasion front would estimate the population to be growing faster—both in absolute terms and relative to generational “growth”—than demographically accurate, because of dispersal from previously colonized habitat.

An important assumption of spreading speed calculations is that of linear predictability, that is, that low-density projection matrix  $\mathbf{A}$  determines the rate at which invasion occurs. In the case of generational spread, the description may not be strictly accurate, given that  $\mathcal{L}_G$  operates across time steps as invasion or recolonization advances, and multiple generations grow simultaneously. Still, we might hope to approximate the rate of spread for the true nonlinear dynamics by considering regions of space at the far front of the invasion (near  $\mathbf{u} = 0$ ) so that  $\mathbf{A}$  will adequately project population changes for many time steps. In any case, we have shown how our measure of spreading speed for the linearized generational model (5) relates to spreading speed for the linearized annual model (1), and the link between annual spread in the linear and nonlinear models is well established (Lui 1989a; Neubert and Caswell 2000). We have not addressed the problem of generational spread for a full, nonlinear model of spatial population dynamics, but we have shown how analysis of the linearized form can be useful.

We have dealt with discrete-time difference equations to model population change, as are appropriate for many species. While this is a common approach in the study of population spread (e.g., Neubert and Caswell 2000; Neubert and Parker 2004; Krkošek et al. 2007; Smith et al. 2009), an obvious alternative would be to use continuous-time differential equations. A measure of generational spreading speed may be possible to derive for partial differential equation models, incorporating continuous change in space and time, and this remains an opportunity for future work.

The idealized model we have presented applies to homogeneous landscapes. Others have begun to characterize IDE spreading speeds that incorporate landscape heterogeneity (e.g., Gilbert et al. 2014). Another approach is to characterize source-sink dynamics across heterogeneous environments on a generational timescale, assessing whether environmental patches or the environment as a whole generate  $R_0 > 1$  (Krkošek and Lewis 2010). This second approach does not characterize spatial movement, but it does consider invasion potential, and the calculations take a form similar to that we have presented. The problem of a next-generation analysis of population spread in a heterogeneous landscape remains open.

We have shown how to calculate generational spreading speed for a stage-structured, dispersing population. This can be simpler, yielding an easier-to-interpret result, than calculation of annual spreading speed. Importantly, the generational measure also carries the same information as the annual measure about whether a population will spread in space. Especially in the case of biased dispersal, as in a stream or along a coastline, where population growth does not guarantee population spread, these features make the generational spreading speed a useful tool. By helping to

clarify how life-history parameters influence an organism's ability to spread, calculation and interpretation of the generational spreading speed could help to identify controls for invasive species or actions to facilitate successful reintroduction. Here, the concept of a generational invasion "wave" is a useful heuristic, although we could not actually measure a generation of individuals spread out through time. This fact is no less relevant in the case of population-level growth, and the concept of the generational growth rate,  $R_0$ , has proven useful across ecological and epidemiological fields (Cushing and Yicang 1994; Caswell 2001; Heesterbeek 2002; de-Camino-Beck and Lewis 2008; Krkošek and Lewis 2010). We expect the concept of generational spreading speed to do the same in the context of biological (re)invasions.

### Acknowledgments

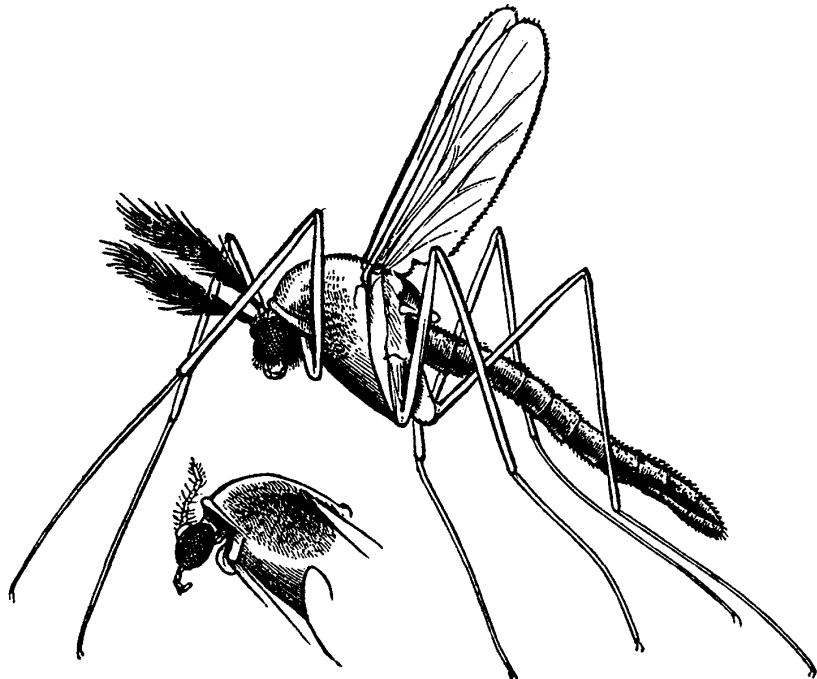
We thank A. Butenschön, K. Erickson, and N. Marculis for their contributions to a similar green crab model and T. Tinker for kindly providing sea otter dispersal data that informed our discussion. Support for this work was provided, in part, by a postdoctoral fellowship (A.W.B.), Discovery Grants (M.K., M.A.L.), and an Accelerator Grant (M.A.L.) from the Natural Sciences and Engineering Research Council of Canada. The material is based on work supported by the US National Science Foundation under grants DEB-1145017 and DEB-1257545 to M.G.N. M.A.L. also received support from the Canada Research Chair program and a Killam Research Fellowship.

### Literature Cited

- Audet, D., D. Davis, G. Miron, and M. Moriyasu. 2003. Geographical expansion of a nonindigenous crab, *Carcinus maenas* (L.), along the Nova Scotian shore into the southeastern Gulf of St. Lawrence, Canada. *Journal of Shellfish Research* 22:255–262.
- Berrill, M. 1982. The life cycle of the green crab *Carcinus maenas* at the northern end of its range. *Journal of Crustacean Biology* 2:31–39.
- Bullock, J. M., S. M. White, C. Prudhomme, C. Tansey, R. Perea, and D. A. P. Hooftman. 2012. Modelling spread of British wind-dispersed plants under future wind speeds in a changing climate. *Journal of Ecology* 100:104–115.
- Caswell, H. 2001. Matrix population models: construction, analysis, and interpretation. Sinauer, Sunderland, MA.
- Clark, J. 1998. Why trees migrate so fast: confronting theory with dispersal biology and the paleorecord. *American Naturalist* 152: 204–224.
- Cushing, J., and Z. Yicang. 1994. The net reproductive value and stability in matrix population models. *Natural Resource Modeling* 8: 297–333.
- de-Camino-Beck, T., and M. Lewis. 2007. A new method for calculating net reproductive rate from graph reduction with applications to the control of invasive species. *Bulletin of Mathematical Biology* 69:1341–1354.
- . 2008. On net reproductive rate and the timing of reproductive output. *American Naturalist* 172:128–139.
- . 2009. Invasion with stage-structured coupled map lattices: application to the spread of scentless chamomile. *Ecological Modelling* 220:3394–3402.
- Elton, C. 1958. The ecology of invasions by plants and animals. Methuen, London.
- Fagan, W., M. Lewis, M. G. Neubert, and P. van den Driessche. 2002. Invasion theory and biological control. *Ecology Letters* 5: 148–157.
- Fisher, R. 1937. The wave of advance of advantageous genes. *Annals of Eugenics* 7:355–369.
- Gilbert, M. A., S. M. White, J. M. Bullock, and E. A. Gaffney. 2014. Spreading speeds for stage structured plant populations in fragmented landscapes. *Journal of Theoretical Biology* 349:135–149.
- Heesterbeek, J. 2002. A brief history of  $R_0$  and a recipe for its calculation. *Acta Biotheoretica* 50:189–204.
- Kanary, L., J. Musgrave, and R. Tyson. 2014. Modelling the dynamics of invasion and control of competing green crab genotypes. *Theoretical Ecology* 7:391–406.
- Kot, M., M. Lewis, and P. van den Driessche. 1996. Dispersal data and the spread of invading organisms. *Ecology* 77:2027–2042.
- Krkošek, M., J. Lauzon-Guay, and M. Lewis. 2007. Relating dispersal and range expansion of California sea otters. *Theoretical Population Biology* 71:401–407.
- Krkošek, M., and M. Lewis. 2010. An  $R_0$  theory for source-sink dynamics with application to *Dreissena* competition. *Theoretical Ecology* 3:25–43.
- Leroux, S., M. Larrivée, V. Boucher-Lalonde, A. Hurford, J. Zuloaga, J. Kerr, and F. Lutscher. 2013. Mechanistic models for the spatial spread of species under climate change. *Ecological Applications* 23: 815–828.
- Lewis, M., M. Neubert, H. Caswell, J. Clark, and K. Shea. 2006. A guide to calculating discrete-time invasion rates from data. Pages 169–192 in M. W. Cadotte, S. McMahon, and T. Fukami, eds. *Conceptual ecology and invasion biology: reciprocal approaches to nature*. Springer, Dordrecht.
- Li, C., and H. Schneider. 2002. Applications of Perron-Frobenius theory to population dynamics. *Journal of Mathematical Biology* 44:450–462.
- Lubina, J., and S. Levin. 1988. The spread of a reinvading species: range expansion in the California sea otter. *American Naturalist* 131:526–543.
- Lui, R. 1989a. Biological growth and spread modeled by systems of recursions. I. Mathematical theory. *Mathematical Biosciences* 93: 269–295.
- . 1989b. Biological growth and spread modeled by systems of recursions. II. Biological theory. *Mathematical Biosciences* 93:297–312.
- Lutscher, F. 2007. A short note on short dispersal events. *Bulletin of Mathematical Biology* 69:1615–1630.
- Lutscher, F., R. Nisbet, and E. Pachepsky. 2010. Population persistence in the face of advection. *Theoretical Ecology* 3:271–284.
- Lutscher, F., E. Pachepsky, and M. Lewis. 2005. The effect of dispersal patterns on stream populations. *SIAM Review* 47:749–772.

- Mason, S. 1953. Feedback theory—some properties of signal flow graphs. *Proceedings of the IRE* 41:1144–1156.
- Meyer, C. D. 2015. Continuity of the Perron route. *Linear and Multilinear Algebra* 63:1332–1336.
- Miller, T., A. Shaw, B. Inouye, and M. Neubert. 2011. Sex-biased dispersal and the speed of two-sex invasions. *American Naturalist* 177:549–561.
- Neubert, M. G., and H. Caswell. 2000. Demography and dispersal: calculation and sensitivity analysis of invasion speed for structured populations. *Ecology* 81:1613–1628.
- Neubert, M. G., and I. M. Parker. 2004. Projecting rates of spread for invasive species. *Risk Analysis* 24:817–831.
- Parker, I. 2000. Invasion dynamics of *Cytisus scoparius*: a matrix model approach. *Ecological Applications* 10:726–743.
- Potapov, A., and M. Lewis. 2004. Climate and competition: the effect of moving range boundaries on habitat invasibility. *Bulletin of Mathematical Biology* 66:975–1008.
- Pringle, J. 2011. Asymmetric dispersal allows an upstream region to control population structure throughout a species' range. *Proceedings of the National Academy of Sciences of the USA* 108: 15288–15293.
- Rector, B., V. Harizanova, and R. Sforza. 2006. Prospects for biological control of teasels, *Dipsacus* spp., a new target in the United States. *Biological Control* 36:1–14.
- Rueffler, C., and J. Metz. 2013. Necessary and sufficient conditions for  $R_0$  to be a sum of contributions of fertility loops. *Journal of Mathematical Biology* 66:1099–1122.
- Shea, K., and D. Kelly. 1998. Estimating biocontrol agent impact with matrix models: *Carduus nutans* in New Zealand. *Ecological Applications* 8:824–832.
- Smith, C. A., I. Giladi, and Y.-S. Lee. 2009. A reanalysis of competing hypotheses for the spread of the California sea otter. *Ecology* 90: 2503–2512.
- Tinker, M., D. Doak, and J. Estes. 2006. Incorporating diverse data and realistic complexity into demographic estimation procedures for sea otters. *Ecological Applications* 16:2293–2312.
- . 2008. Using demography and movement behavior to predict range expansion of the southern sea otter. *Ecological Applications* 18:1781–1794.
- Weinberger, H. 1982. Long-time behavior of a class of biological models. *SIAM Journal on Mathematical Analysis* 13:353–396.
- . 1975a. The biology of Canadian weeds. 12. *Dipsacus sylvestris* Huds. *Canadian Journal of Plant Science* 55:783–794.
- Werner, P. 1975b. A seed trap for determining patterns of seed deposition in terrestrial plants. *Canadian Journal of Botany* 53:810–813.
- Werner, P., and H. Caswell. 1977. Population growth rates and age versus stage-distribution models for teasel (*Dipsacus sylvestris* Huds.). *Ecology* 58:1103–1111.
- Zhang, R., E. Jongejans, and K. Shea. 2011. Warming increases the spread of an invasive thistle. *PLoS ONE* 6:1–6.

Associate Editor: C. Jessica E. Metcalf  
Editor: Susan Kalisz



"A year ago in August, while dredging in Salem harbor, we detected the larvae of a species of fly living on the floating eel-grass, and apparently living on the vegetable matter collected on it. The twentieth of September they transformed into pupæ . . . , and on the ninth of October appeared the fly [pictured], the male of which has beautifully pectinated antennæ, and belongs to the genus *Chironomus*." From "Natural History Miscellany: Zoölogy" (*The American Naturalist*, 1868, 2:277–279).